 sciendo

Study of a Compton backscattering wall defects detection device using the Monte Carlo method

Xuan Qin,
Jianbo Yang,
Zhengcong Du,
Jie Xu,
Rui Li,
Hui Li,
Qi Liu

Abstract. In view of the shortcomings of traditional wall defect detection methods, such as small detection range, poor accuracy, non-portable device, and so on, a wall defects detection device based on Compton backscattering technology is designed by Monte Carlo method, which is mainly used to detect the size and location information of defects in concrete walls. It mainly consists of two parts, the source container and the detection system: first, through the simulation and analysis of the parameters such as the receiving angle of the backscattered particles and the rear collimating material of the detector, the influence of the fluorescent X-ray peak of the detector collimating material on the backscattered particle counts is eliminated and the detected error is reduced; second, the ring array detector design, compared with single array detector and surface array detector, can facilitate real-time detection of defect orientation, expanding the single scan range and improving the detection efficiency. After simulation and comparative analysis, the relevant optimal parameters are obtained: the object is detected using a Cs-137 γ-ray source with an activity of 6 mCi, and a ring detector consisting of four 0.5-inch cube-shaped CsI scintillator detectors is placed at 150° to receive the backscattered photons. The simulation analysis using the Monte Carlo FLUKA program showed that the maximum depth of wall defect detection is 8 cm, the maximum error fluctuation range of defect depth and thickness is ±1 cm, the overall device weight is <20 kg, and the measurement time is <5 min.

Keywords: Compton backscattering • Monte Carlo • Nondestructive testing • Wall defects

X. Qin, J. Xu, R. Li, H. Li
Chengdu University of Technology
Chengdu, Sichuan 610059, China

J. B. Yang✉
Chengdu University of Technology
Chengdu, Sichuan 610059, China
and Sichuan University of Science & Engineering
Zigong, Sichuan 643000, China
E-mail: yjb@cdut.edu.cn

Z. C. Du
Xichang University
Xichang, Sichuan 615000, China

Q. Liu
Sichuan University of Science & Engineering
Zigong, Sichuan 643000, China

Introduction

With the rapid development of social economy, the demand for buildings is expanding; however, the buildings are prone to defects in the process of construction and use. Once there are defects in the interior of the building wall, these will affect its safety, load-bearing capacity, and durability, resulting in serious casualties and property losses. Therefore, it is necessary to detect the defects in the wall and prevent potential safety hazards.

At present, the commonly used wall defect detection methods include the visual inspection, infrared thermal imaging [1, 2], impact echo [3, 4], pulse response [5], and ultrasonic nondestructive testing [6] methods. The visual inspection method is greatly influenced by subjectivity [1]; the infrared thermal imaging method takes a long time, and the imaging effect is strongly dependent on the external temperature and the smoothness of the wall surface [7]; the impact echo method cannot provide accurate information on certain aspects such as the location and size of defects [8, 9]; and the ultrasonic nondestructive testing method requires calibration in combination with a large number of data condi-

tions, and without calibration curves, the results are unreliable [10, 11].

As an imaging technique that measures the Compton backscattered lines radiated by the irradiated object, the main advantage of the Compton backscattering technique is that it employs one-side, non-contact detection; and accordingly, it has been applied in detection-oriented functionalities in the following classes of contraption, among others: solid rocket motor [12], external insulation system of building exterior walls [13], mild steel (to gauge the degree of concealed internal corrosion) [14], thickness measurement of thin material plate [15], and pipeline (for corrosion detection on the interior surface) [16]. It also shows good application potential in concrete defect detection. In 2003, Wu [17] used a 100 Ci Ir-192 radiation source and an NaI(Tl) detector to carry out nondestructive testing to verify whether the density of reinforcement in the wall meets the established quality standards. The results showed that reinforcement with a diameter of >2 mm within 10 cm of the wall can be detected. In 2014, Boldo and Appoloni [18] used a 100 mCi Am-241 radiation source and a CdTe detector to conduct nondestructive testing on the hidden corrosion inside the reinforcement. The results showed that steel inclusions and defects with a radius of 4 mm within 2 cm from the sample surface could be detected. In 2019, Sari *et al*. [19] compared and analyzed the detection effects of Co-60 and Cs-137 radiation sources on cavities in concrete volume. The results showed that Cs-137 radiation source is more effective in the Compton scattering nondestructive testing system. However, in the above examples, the overall device is too large, the weight is too heavy, and the detection range is too small. In addition, the staffs need to be >2 m away from the source container in actual operation, which cannot meet the requirements of portability and deep detection range of the device at the same time.

Therefore, a wall defect detection device based on Compton backscattering technology is proposed in this paper. The structures are designed and optimized by the Monte Carlo program, which is widely used in the nuclear field [20]. Through the simulation and analysis of the structure and size of the source container, the angle at which the detector receives backscattered particles, the rear collimating material of the detector and other parameters, and the optimal device parameters that meet the requirements are obtained.

Simulation model

The interaction of X-rays or γ-rays with the orbital electrons or free electrons in the atomic shell of the specimen will cause electrons to recoil, at which time the incident photons with reduced energy will propagate in a new direction, a phenomenon referred to as Compton scattering [12]. Compton backscattering refers to the Compton scattering in which the exit angle of scattered photons is >90°. In the Compton backscattering effect, the scattering intensity is roughly proportional to the density

of the material. The size of the shape of the defect within the wall and the location of its presence can be determined by comparing the number of Compton backscattered particles received by the detector.

The overall structure of the Compton backscattering wall defect detection device, which mainly consists of a source container system and a detector system, is shown in Fig. 1. The source container system consists of a hollow lead sphere radiation source container with an inner diameter of 0.8 cm and an outer diameter of 3.1 cm and a lead front collimator with an inner diameter of 0.5 cm; each component is covered with a stainless steel shell with a thickness of 0.3 cm as the structural support material. A cylindrical Cs-137 radioactive source with an inner diameter of 0.4 cm and a height of 1 cm was placed in the center of a hollow lead sphere. The detector system consists of four 0.5-inch CsI array detectors and a copper rear collimation with an aperture of 0.885 cm. Four detectors are used to detect defects in four directions relative to the source container: up, down, left, and right; two detectors for detecting the up and down directions; and two detectors for detecting the left and right directions, each constituting one detection unit; that is, four detectors are used for two detection units, in total constituting one group of ring array detectors. In this work, ordinary concrete containing O, Si, Ca, H, Al, Na, K, Fe, C, and Mg is used as the main object of study, which corresponds to the following percentages of elements contained: 57.5, 30.5, 4.3, 2.2, 2.0, 1.5, 1.0, 0.6, 0.3, and 0.1%. The distance of the upper surface of the defect in the concrete structure from the detection surface is defined as the depth of the defect. We simulate the cylindrical defects with a hole diameter range of 1–3.5 cm, a thickness range of 1.5–5.5 cm, and a depth range of 0–8 cm, moving the defect detection device with a fixed detection step of 0.5 cm in the y-axis direction, and utilizing the obtained data to analyze the size and location of the defects. We fix the distance between the radioactive source and the concrete wall, and avoid the location of the source container system, placing the detector at a direction of 105–180° relative to the incident beam direction, and using the USRTRACK
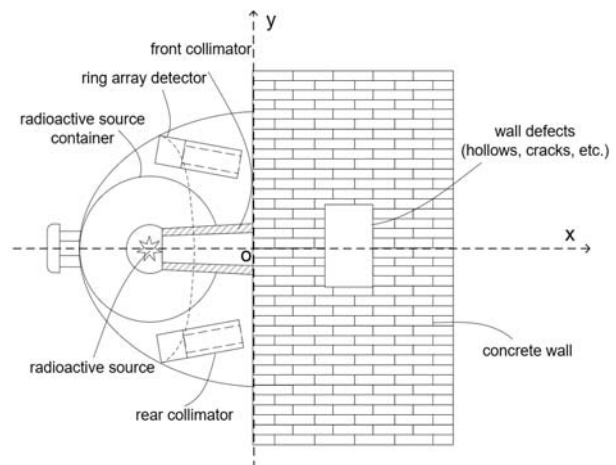
Fig. 1. Schematic diagram of Compton backscattering wall defect detection device.

record card in the Monte Carlo FLUKA program [21] to obtain the backscattered energy spectrum information as well as the best detector reception angle to maximize the use of space and source particles.

The present study endeavors to ensure prevalence of the following conditions: the ray incident direction is set as the x-axis positive direction, and the vertical ray incident direction is set upward as the y-axis positive direction for subsequent description.

Results and discussion

The determination of the detection range and the selection of the angle at which the detector receives backscattered particles

As shown in Fig. 1, we take the concrete wall with the same cross section and different thickness as the scatterer, fix the distance between the radiation source and the scatterer, distribute the detector on a quarter circle close to the direction of the source container, and calculate the area of the backscattering peaks under different detection angles; and the obtained results are shown in Fig. 2. It can be seen from Fig. 2 that the area of backscattering peak increases with the increase of concrete thickness, but it does not increase infinitely. When the thickness of concrete reaches 8 cm, the backscattered rays are absorbed in a large amount, and the area of backscattering peak changes slowly and gradually tends to saturate. At this time, the thickness is called the saturated thickness of the concrete. When the wall defect is outside the saturated thickness of the concrete, the change in the number of particles received by the detector is easily submerged by the noise caused by various uncertain factors in the actual detection, and the effect of detecting and imaging the wall defects cannot be achieved. Therefore, the detection range of the wall defect of the device is limited to 8 cm from the lower surface of the defects to the detection surface of the concrete.

The selection of receiving backscattered particles' angle is the key part of the detection system design. The trend of the backscattering peak area with the
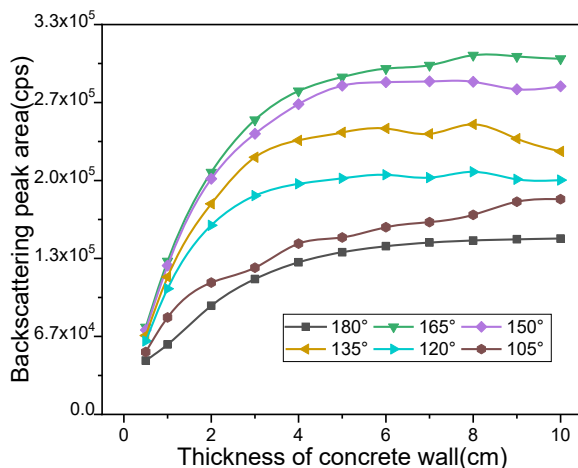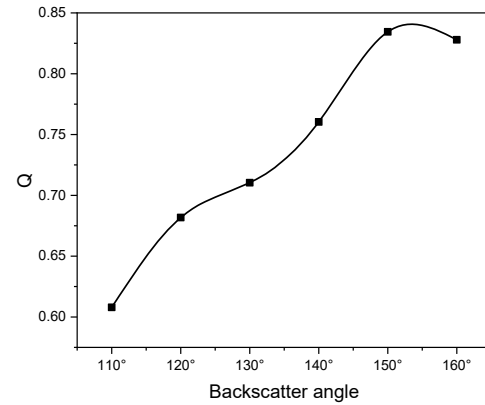
Fig. 3. Effect of backscattering angle on scattering element volume and backscattering peak area.

angle is variously simulated in steps of 15° for the range of backscattering angle of 105–180°, and it can be seen from Fig. 2 that the number of backscattered particles increases with the increase of angle, except for 180°, which is completely opposite to the direction of incident particles. After calculation, in this model, the angle at which the backscattered rays avoid the shielding of the source container should be <160°.

In this paper, the volume element cut from the intersection of the front collimation of the radioactive source container and the rear collimation of the detector system is called the scattering element. The model shows that the volume of the scattering element is different at different detection angles, which has an impact on the defect detection efficiency of the device. Also varying with the detection angle is the backscattered peak area received by the detector. In order to consider the effects of the two variations simultaneously, this paper normalizes the two variations of scattering angle-scattering element volume and scattering angle-backscattering peak area curves in the range of backscattering angle <160° in steps of 10°. The normalized curves are multiplied together, and the results are shown in Fig. 3.

In Fig. 3, the horizontal axis is the backscattering angle, and the vertical axis is the product of the scattering element volume and the backscattering peak area, which is expressed by Q. It is dimensionless, and the significance is to measure the effect of the backscattering angle on the scattering element volume as well as the backscattering peak area at the same time. As can be seen in Fig. 3, the Q value increases and then decreases with the increase of the backscattering angle within the detection range that meets the requirements of this model, and the turning point is located in the interval around 150°. Therefore, in order to ensure the detection efficiency and maximize the utilization of source particles, the detection crystal is placed at a scattering angle of 150°.

Selection of rear collimating material

In order to improve the detection intensity of backscattered rays and reduce the interference of backscattered rays between different measurement units, the changing relationship of energy spectrum is simulated

Fig. 2. Variation of backscattering peak area with detection angle and thickness of concrete wall.
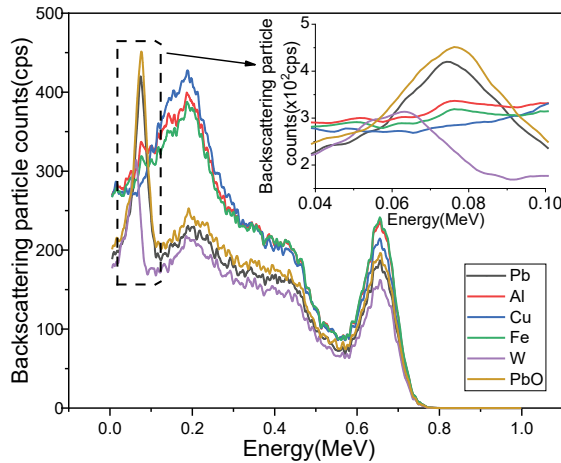
Fig. 4. Energy spectrum of different detector rear collimating materials.

Fig. 5. Example diagram for defect orientation detection of symmetrical distribution detector.

and studied when Pb, Fe, W, Cu, and other materials are used as the rear collimating materials of the detector. The results are shown in Fig. 4. It can be seen from Fig. 4 that when other materials except Cu are used as rear collimator, there are fluorescent X-ray peaks around 70 keV in the energy spectrum, which have an impact on the counting of backscattering peak areas. Because the Compton backscattering signal is weak, the existence of fluorescence X-ray peaks will cause great error in the results, and when Cu is used as the rear collimating material, the backscattering peak counts are the highest and the peak area counts are the largest, and so Cu is selected as the rear collimating material of the detector.

Ring array detector design

It is not easy to determine the defects in a concrete wall using merely the naked eyes; coupled with the existence of quantum noise, it is necessary to ensure the single detection time in order to accurately distinguish the wall defects. If the defects can be roughly located and the detection range can be reasonably planned during the inspection process, the overall detection speed can be improved.

The defect orientation detection process is shown in Fig. 5; in this device, symmetrically distributed detectors are used to detect defects, and the present study adopts the following procedure for this purpose: the ray incident direction is taken as the boundary, and since the backscattered rays detected by the detector located in the positive half axis of the y-axis mainly come from the defects in the negative half axis of the y-axis, it is set as a negative detector. Similarly, the detector located on the negative half axis of the y-axis is set as the positive detector. We fix the size of the defect, move the ring array detector in the y-axis direction to detect the defect, and analyze the situation when the defect is located at different depths. As the defect detection depth increases, the amount of backscattered particles received by the detector becomes less and less, the quantum noise ratio increases, and the effective signal ratio decreases [22]. To achieve the goal of detecting defects at deeper locations, the ratio method is used here to eliminate the effect of quantum noise and emphasize the change in the effective signal. Compared with the ratio calculation using the result value of the count without defects as the reference group, the ratio calculation using the result value of the count with any known defect size and position as the reference group can predict the size and position of the defects based on the change in the number of backscattered particles, which would in turn be based on the orientation judgment, and reasonably set the detection range according to the magnitude of the change combined with the presetting algorithm. In this study, the detection value of the defect located at 0.5 cm depth with a radius of 0.8 cm is used as an example of the reference group, and the defects with a radius of 1 cm and depths of 1 cm, 4 cm, and 7 cm are analyzed, the results of which are shown in Fig. 6.
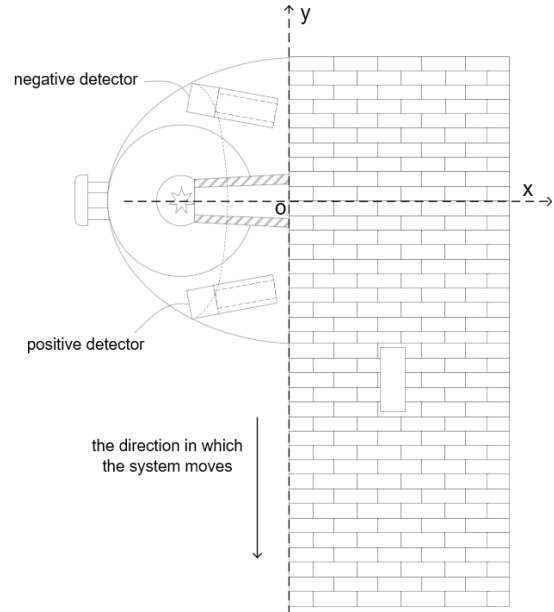
It can be seen from Fig. 6 that these curves have the same trend regardless of the distance between the wall defects' surface and the detection surface. If analyzing from left to right: at the beginning of detection, the wall defect is located below the detector. In the first period of time, the wall defect did not enter the detection range of any detector, and so the counting of the positive and negative detectors is in a relatively stable state, as shown in area I in the figure. When the detector gradually approaches the location of the defect, the wall defect first enters the detection range of the negative detector. At this time, the ratio of the negative detector will fluctuate compared with the positive detector, as shown in area II in the figure. With the movement of the detector, the volume of wall defects entering into the negative detector detection range increases and begins to enter the detection range of the positive detector, and at this time the ratio of both positive and negative detectors will have a large fluctuation, as shown in area III in the figure. When the detector gradually moves away from the loca-
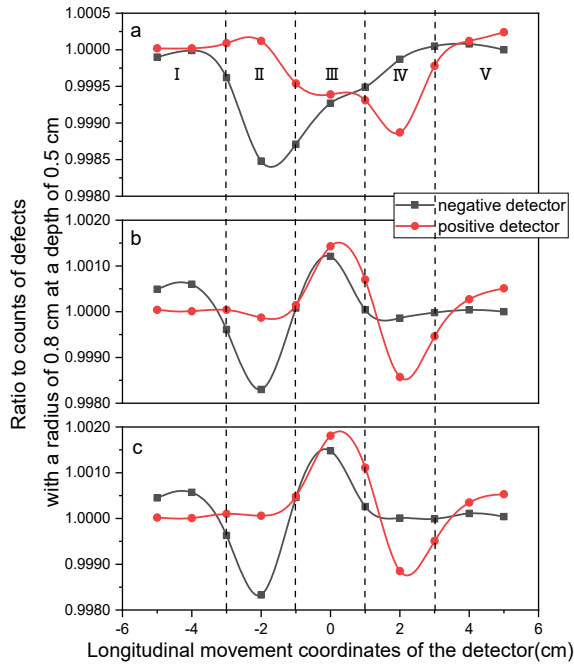
Fig. 6. The use of ring array detectors in the determination of the direction of defects: the depth of the defect is, variously: (a) 1 cm, (b) 4 cm, and (c) 7 cm.

tion of the defect, the wall defect gradually emerges out of the detection range of the negative detector, and thereafter only exists in the detection range of the positive detector. At this time, the ratio of the positive detector will fluctuate compared with the negative detector, as shown in area IV in the figure. Finally, the wall defect will gradually move away from the detection range of any detector, and the counts of the two detectors will be in a relatively stable state again, as shown in area V in the figure. Therefore, if area II occurs in the measurement, it indicates that the defect exists only in the detection range of the negative detector. All that is needed is to move along the detection range of the negative detector to reach the location of the defect. If area III occurs in the measurement, it indicates that the defect exists in the detection range of both positive and negative detectors, whose size and position will increase the number of backscattered particles compared to the reference group, and the size and position of the defect can be predicted according to its variation and combined with the presetting algorithm to improve the overall detection speed.

Determination of cross-sectional size, thickness, and depth of defects in the wall

The objectives of the detection of defects include the cross-sectional size of the defect, the thickness of the defect, and the depth at which the defect is located. To begin with, the cross-sectional size of the defect is judged. The effect of simulating wall defects models with different cross-sectional sizes is shown in Fig. 7. Under the same conditions, the larger the cross section of the defect, the less the number of particles received, and the more obvi-
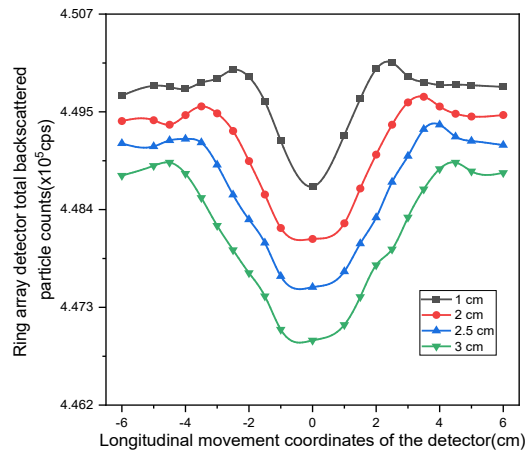
Fig. 7. Variation of backscattered particle counts with different cross-sectional radius of defects.

ous the change range. The defects simulated in this model are several cylinders with a radius of 1–3 cm. Taking 0.5 cm as the detection step, the detection counts of the detector are displayed in the range of $r = 2.5$–4.5 cm. The simulation results have the same variation law as the set defect radius, and the difference is constant at the same depth.

When the device is used to determine the thickness and depth of defects, the two parameters are closely related. We fix the cross-sectional area of the defects, change the depth and thickness of the defects for simulation, and calculate the ratio between the simulation results and the number of backscattered particles received in the defect-free state. The effect is shown in Fig. 8.

It can be seen from the figure that the counting of backscattered particles at a certain position mainly depends on the depth of the defect at the current position and the thickness of the defect in the direction of the incident ray, and has little to do with the cross-sectional area of the defect under the current condition. When the position of the defects exceeds the saturated thickness of the concrete wall, with the deepening of the defects' depth, the corresponding curve will tend to coincide with the curve with thinner defect thickness at the same depth,
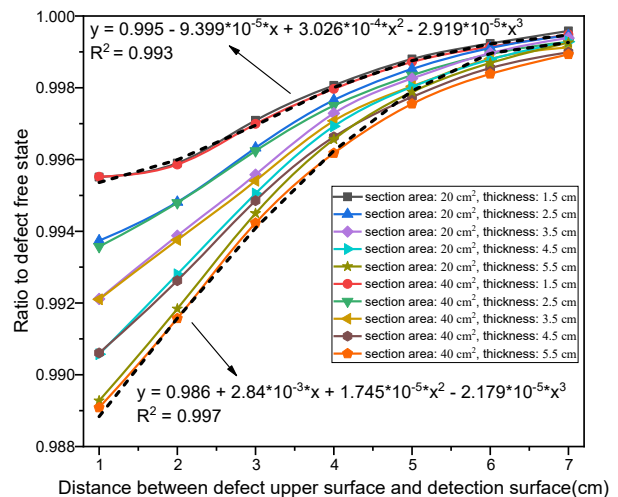
Fig. 8. Determination of defect thickness and depth.

that is, when the defect thickness at a certain depth increases beyond the saturated thickness of the concrete, the contribution of the part exceeding the saturated thickness to the overall counts will gradually decrease. Therefore, only the defects located completely inside the saturated thickness of the concrete walls are analyzed and discussed here. Excluding the data other than the saturated thickness in Fig. 8, we fit the data into two cubic curves with correlation coefficients >0.99, within which the maximum error fluctuation range for the detection of defect depth as well as thickness was ±1 cm.

Conclusion

The main conclusions obtained from the simulations in this work are as follows: (1) cube-shaped CsI scintillator detectors having each a size of 0.5 inch and arranged into multiple arrays are used as the detection crystal, and the particles received in the direction of the backscattering angle of 150° are counted. Each CsI crystal is combined with Cu as a rear collimation material to form one detector, two detectors to form one detector unit, and four detectors to form two detector units as a ring array detector, which can facilitate real-time detection of defect orientation; (2) when testing the defect cross-sectional radius, the simulation results have the same variation law as the set defect radius, and the difference is constant at the same depth; (3) the maximum error fluctuation range of defect depth and thickness detection is ±1 cm. The simulation results show that the results can better meet the design requirements of the device, but further optimization and improvement are needed to achieve more accurate analysis of the thickness and depth of defects.

ORCID

J. B. Yang http://orcid.org/0000-0001-8429-5018

References

1. Ge, J. Y., & Hou, J. L. (2021). Research on defects of building exterior wall based on infrared thermal imaging technology. In 27th Annual Academic Conference of Beijing Society of Theoretical and Applied Mechanics, 16 January 2021 (pp. 1122–1124). Beijing, China: Beijing Society of Theoretical and Applied Mechanics. (in Chinese).

2. Jin, H., & Zou, L. L. (2021). Detection of hidden disease of concrete bridge based on infrared thermal imaging. *J. Phys.-Conf. Series, 1748*(4), 042041. DOI: 10.1088/1742-6596/1748/4/042041.

3. Yao, F., Lu, X. Q., & Chen, G. Y. (2021). Experimental and signal processing research on concrete-rock structural defects by impact-echo method. *Journal of Railway Science and Engineering, 18*(9), 2316–2323. DOI: 10.19713/j.cnki.43-1423/u.T20200974. (in Chinese).

4. Yeh, P. L., Liu, P. L., & Hsu, Y. Y. (2018). Parametric analysis of the impact-echo phase method in the differentiation of reinforcing bar and crack signals. *Constr. Build. Mater., 180*, 375–381. DOI: 10.1016/j.conbuildmat.2018.05.243.

5. Zheng, H., & Kappatos, V. (2015). Defect detection in concrete pile using impulse response measurements with sine sweep excitations. In International Symposium Non-Destructive Testing in Civil Engineering, 15–17 September 2015 (pp. 1–4). Berlin, Germany: Federal Institute for Materials Research and Testing.

6. Lee, T., & Lee, J. (2020). Setting time and compressive strength prediction model of concrete by nondestructive ultrasonic pulse velocity testing at early age. *Constr. Build. Mater., 252*, 119027. DOI: 10.1016/j.conbuildmat.2020.119027.

7. Yang, H. L. (2022). Feasibility study on detecting internal damage of concrete after fire by impact echo method. *Industrial Technology & Vocational Education, 20*(1), 11–16. DOI: 10.16825/j.cnki.cn13-1400/tb.2022.01.003. (in Chinese).

8. Niu, C. (2017). *Principle study on detection of void condition behind tunnel lining by hammering method*. Masteral dissertation, Beijing Jiaotong University, Beijing, China. (in Chinese).

9. Zhao, Q., Sang, Y., Gao, J. L., Yang, Y. Z., Sui, L. Z., & Zhu, W. Z. (2019). Summary of the research on impact-echo method to evaluate the quality of concrete. *China Concrete and Cement Products, 12*, 18–23. DOI: 10.19761/j.1000-4637.2019.12.018.06. (in Chinese).

10. Trtnik, G., Kavčič, F., & Turk, G. (2009). Prediction of concrete strength using ultrasonic pulse velocity and artificial neural networks. *Ultrasonics, 49*(1), 53–60. DOI: 10.1016/j.ultras.2008.05.001.

11. Solís-Carcaño, R., & Moreno, E. I. (2008). Evaluation of concrete made with crushed limestone aggregate based on ultrasonic pulse velocity. *Constr. Build. Mater., 22*(6), 1225–1231. DOI: 10.1016/j.conbuildmat.2007.01.014.

12. Lin, D. F., Chen, Z. H., Liu, M. M., Jia, Q. L., & Liu, L. H. (2017). Application of Compton backscattering technique in SRM detection. *Nondestructive Testing, 39*(12), 51–53. DOI: 10.11973/wsjc201712012. (in Chinese).

13. Wang, Z. L., Zhang, D. B., Li, X. M., Jiang, L. X., Chen, X. & Li, Y. S. (2020). Research on Compton back-scatter scanning detection technology for external wall thermal insulation system of existing buildings. *Construction Technology, 49*(9), 9–11+19. DOI: CNKI:SUN:SGJS.0.2020-09-003. (in Chinese)

14. Margret, M., Menaka, M., Subramanian, V., Baskaran, R., & Venkatraman, B. (2018). Non-destructive inspection of hidden corrosion through Compton

backscattering technique. *Radiat. Phys. Chem., 152,* 158–164. DOI: 10.1016/j.radphyschem.2018.07.015.

15. Chuong, H. D., Thong, N. D., Nguyen, V. H., Minh, L. H., Truc Linh, N. T., Ho, P. L., Thanh, T. T., & Van Tao, C. (2022). Non-destructive evaluation of thickness of material plates through Compton backscattering technique using Si(Li) detector. *Radiat. Phys. Chem., 193,* 109978. DOI: 10.1016/j.radphyschem.2022.109978.

16. Jamshidi, V., & Davarnejad, R. (2021). Photon backscatter radiography application for the simulation of corrosion detection inside a pipeline: A novel proposal for 360° corrosion consideration in the pipelines. *Appl. Radiat. Isot., 176,* 109844. DOI: 10.1016/j.apradiso.2021.109844.

17. Wu, J. Z. (2003). *Portable Compton backscatter imager study.* Masteral dissertation, Zhejiang University, Zhejiang, China. (in Chinese).

18. Boldo, E. M., & Appoloni, C. R. (2014). Inspection of reinforced concrete samples by Compton backscattering technique. *Radiat. Phys. Chem., 95,* 392–395. DOI: 10.1016/j.radphyschem.2012.12.013.

19. Sari, M. B., Wirawan, R., Waris, A., Kim, H. J., & Djamal, M. (2019). Simulation of void detection system using gamma-ray Compton scattering technique. *J. Eng. Technol. Sci., 51*(3), 369–379. DOI: 10.5614/j.eng.technol.sci.2019.51.3.5.

20. Zhang, C., Yang, J., Li, R., Qiao, Y., Zhang, X., & Xu, J. (2020). Fluka simulation of PGNAA system for determining heavy metal pollution in the soil sample. *Nukleonika, 65*(1), 13–17. DOI: 10.2478/nuka-2020-0002.

21. Ferrari, A., Sala, P. R., Fasso, A., & Ranft, J. (2005). *Fluka: A multi-particle transport code.* United States: U.S. Department of Energy Office of Scientific and Technical Information.

22. Cao, Y. N. (2010). *Compton scattering imagining technique in nondestructive test of aircraft structures research and simulation.* Masteral dissertation, Civil Aviation University of China, Tianjin, China. (in Chinese).